HOKKAIDO UNIVERSITY

Title	Exploring the Reaction Mechanism of Heterobimetallic Nickel-Alkali Catalysts for Ethylene Polymerization : Secondary-Metal-Ligand Cooperative Catalysis
Author(s)	Apilardmongkol, Pavee; Ratanasak, Manussada; Hasegawa, Jun-ya; Parasuk, Vudhichai
Citation	ChemCatChem, 14(13), e202200028 https://doi.org/10.1002/cctc.202200028
Issue Date	2022-07-07
Doc URL	http://hdl.handle.net/2115/90136
Rights	This is the peer reviewed version of the following article: P. Apilardmongkol, M. Ratanasak, J.-y. Hasegawa, V. Parasuk, ChemCatChem 2022, 14, e202200028., which has been published in final form at https://doi.org/10.1002/cctc.202200028. This article may be used for non-commercial purposes in accordance with Wiley Terms and Conditions for Use of Self-Archived Versions. This article may not be enhanced, enriched or otherwise transformed into a derivative work, without express permission from Wiley or by statutory rights under applicable legislation. Copyright notices must not be removed, obscured or modified. The article must be linked to Wiley ’ s version of record on Wiley Online Library and any embedding, framing or otherwise making available the article or pages thereof by third parties from platforms, services and websites other than Wiley Online Library must be prohibited.
Type	article (author version)
File Information	ChemCatChem_paper.pdf

Instructions for use

Hokkaido University Collection of Scholarly and Academic Papers : HUSCAP

RESEARCH ARTICLE

Exploring the Reaction Mechanism of Heterobimetallic Nickel-Alkali Catalysts for Ethylene Polymerization: Secondary-Metal-Ligand Cooperative Catalysis

Pavee Apilardmongkol,[a] Manussada Ratanasak,*[b] Jun-ya Hasegawa,*[b] and Vudhichai Parasuk *[a]

[a] P. Apilardmongkol, Prof. V. Parasuk
Center of Excellence in Computational Chemistry
Department of Chemistry, Faculty of Science, Chulalongkorn University
Pathumwan, Bangkok 10330, Thailand
E-mail: pavee_pongsajanukul@hotmail.com, vudhichai.p@chula.ac.th
[b] Dr. M. Ratanasak, Prof. J. Hasegawa
Institute for Catalysis
Hokkaido University
Kita21, Nishi10, Kita-ku, Sapporo, Hokkaido 001-0021, Japan
E-mail: manussada@cat.hokudai.ac.jp, hasegawa@cat.hokudai.ac.jp

Supporting information for this article is given via a link at the end of the document.

Abstract: In this work, we explored the reaction mechanism of heterobimetallic nickel phenoxyphosphine polyethylene glycol (Ni-PEG) with alkali metals (M^+ = Li^+, Na^+, K^+, and Cs^+) catalysts for ethylene polymerization using the DFT calculations. The activation energy of the necessary step shows the following trend, $Li^+ < Na^+ < K^+ < Cs^+$, which corresponds to experimentally observed activities. Roles of secondary metals (M^+) in Ni-PEG catalysts were clarified. Our findings suggest that the active catalyst should contain strong cooperative metal-metal/metal-ligand interactions and less positive charge on M^+ cation. Besides, the key role of M^+ is to control the PEG group which stabilizes the catalyst structure. In addition, we found two key factors (shorter M-O_1 and M-O_{PEG} distances) for designing new catalysts from the pre-reaction state of the Ni-PEG(M^+) catalysts. Finally, Ni-PEG(M^{2+}) catalysts with Be^{2+}, Mg^{2+}, Co^{2+}, and Zn^{2+} were suggested for candidates of highly active catalysts for ethylene polymerization.

Introduction

Polyethylene (PE) is one of the most used plastic materials in the world. It is useful not only for plastic production but also for various applications. This is due to its unique properties such as flexible, weatherproof, translucent, good low-temperature toughness, excellent chemical resistance, excellent electrical insulating properties, etc. [1]. The trend of world plastics productions by PE is rising in the double for the next 20 years [2]. The heterogeneous Ziegler-Natta (ZN) catalysts [3-4] have been widely used for the industrial production of polyolefin since their invention. However, one of the major drawbacks for this catalytic system is its multiple active sites which are provided by transition metal for olefin insertion [5]. Hence, homogeneous single-site catalysts have been developed to overcome this problem. Many studies have been conducted, and new homogeneous metallocene [6-9] and post-metallocene/non-metallocene [10-14] have been synthesized. New ligands and transition metal centers particularly with group IVB transition metals such as titanium (Ti), zirconium (Zr), and hafnium (Hf) or late transition metals such as nickel (Ni) and palladium (Pd) have been introduced. Nevertheless, continuing efforts are being devoted to these catalysts for improving efficiency.

In the last decade, heterobimetallic catalysts which contain two different metals in a single platform have significantly improved the catalytic reactivity [15-17]. The heterobimetallic catalysts can enhance polymerization reactivity by multiple explicit interactions [18]. The use of two different metals possibly affects the olefin insertion and increases/decreases the rate of polymerization. The advantage of heterobimetallic complexes is a significant enhancement in catalytic activity when compared to monometallic catalysts [19]. The late transition metal catalysts containing either Pd or Ni were introduced as excellent catalysts for ethylene polymerization [20]. Nickel has attracted the most interest, not only because of its higher activities in ethylene polymerization but also less toxicity and better cost efficiency than Pd [21-22]. Moreover, Ni complexes can be utilized with various reagents in the uncomplicated process and inexpensive precursors [23].

The Do group [24] has pioneered the synthesis of nickel complexes supported by phenoxyimine ligands having pendant polyethylene glycol side chains (NiL). They demonstrated that the addition of alkali metal ions (M^+ = Li^+, Na^+, K^+) to NiL can enhance the catalytic performance (up to a 20-fold) for ethylene polymerization as well as enhancement in polymer molecular weight and polymer branching compared to polymerizations performed in the absence of alkali metal ions. This work reflects the beneficial effect of secondary metal ions on metal-catalyzed olefin polymerization processes. Furthermore, they [25] reported that the combination between different nickel catalysts and alkali ions (Na^+ or K^+) provided polyethylene with different branching microstructures and molecular weights. Zhang et al. [26] introduced the installation of a PEG unit that can enhance catalytic activity, catalytic stability, and molecular weight of nickel catalysts. Four ether oxygens of the PEG group provide metal binding sites for the alkali metal which control the architecture of the polymer during ethylene polymerization. As a result, the existence of secondary metals could significantly improve the catalytic activity. In addition, Do group [27] suggested that the platform of phenoxyphosphine ligand connected to the PEG group could be attached by several secondary metals.

Tran, Do and co-workers [28] have designed a new class of heterobimetallic nickel-sodium phenoxyphosphine polyethylene glycol, called Ni-PEG(Na^+) hereafter, for ethylene polymerization. This discovery revealed that the presence of sodium cations could accelerate the rate of polymerization. Only the alkali metal cations have been incorporated into the polyethylene glycol (PEG) group.

In recent years, Tran et al. [29] expanded their investigation of the effects of other alkali ions on Ni-PEG catalysts and demonstrated that Ni-PEG(M^+) exhibited higher activity than monometallic nickel catalysts. This is owing to the steric protection of the M-PEG group on the axial position of nickel. The Ni-PEG with Li^+ as a secondary metal provided the highest activity at moderate temperatures (30-50 °C) followed by Na^+, K^+, and Cs^+. The catalytic performance can be controlled and boosted up by the size of M^+. In the light of Tran's work [29], the mechanistic model for ethylene polymerization catalyzed by Ni-PEG(M^+) and molecular interactions inside Ni-PEG(M^+) complexes are still insufficiently clarified. Furthermore, for further catalyst design, there are several remaining questions, i.e. the function of secondary metals in polymerization, types of interactions that are significant for this catalytic reaction, and the contribution of steric and electronic effects. Hence, it becomes our interest to understand the behavior of the Ni-PEG(M^+) catalysts for ethylene polymerization at the molecular level.

The density functional theory (DFT) calculation has been a powerful tool for understanding the reaction mechanisms of ethylene polymerization [30-32]. Mechanisms of ethylene polymerization catalyzed by transition metal complexes were already proposed by many researchers. For instance, Morokuma group reported a DFT study of nickel diamine complex [33]. Zeller and Strassner investigated the mechanism of ethylene polymerization by nickel salicylaldiminato catalysts [34]. Nozaki group conducted both experimental and theoretical studies on the mechanism of the formation of linear PE catalyzed by palladium phosphine−sulfonate complexes [35-36]. Regarding our research target, the X-ray structures of Ni-PEG(M^+) obtained by Tran et al. [28-29] were used in this study. The structure contains $[B(C_6F_5)_4]^-$ counteranion and explicit solvents. Usually, the counteranion affects catalytic activity by acting as an activator to the metal center, which causes the catalyst to be more active toward ethylene polymerization [37]. However, Laine et al. [38] have examined the effect of the counteranion $[B(C_6F_5)_4]^-$ on the insertion of ethylene to $[Cp_2ZrMe]^+$. They found that the reaction pathway for the PE formation with the counteranion is similar to those without one.

In this study, we proposed a reaction mechanism for ethylene polymerization catalyzed by Ni-PEG with alkali metal (M^+) as depicted in **Scheme 1**. This proposed mechanism is based on information from previous studies [36, 39]. Noda et al. [35] and Nakano et al. [36] investigated the cis/trans isomerization process for the Pd/phosphine-sulfonate system and their results indicated that the cis/trans isomerization process occurs via the Berry's pseudo rotation. We hypothesized that nickel and palladium complexes with asymmetric ligands should undergo similar polymerization mechanisms. Thus, in this work, we proposed the mechanism of Ni-PEG catalysts based on the Pd-catalyst which corresponds to the mechanism suggested by Tran et al. [29]. The *cis* to *trans* isomerization of reactant state is the key step. The ethylene was inserted into the nickel metal center after the reactant π-complex undergoes cis/trans isomerization. In addition, the rotation pattern based on TS_{Iso} structure occurs via penta-coordinate complex and corresponds to that discovered by Ugi et al. [40]. Therefore, we believed that the mechanism of cis/trans isomerization in our work occurs via the Berry pseudorotation.

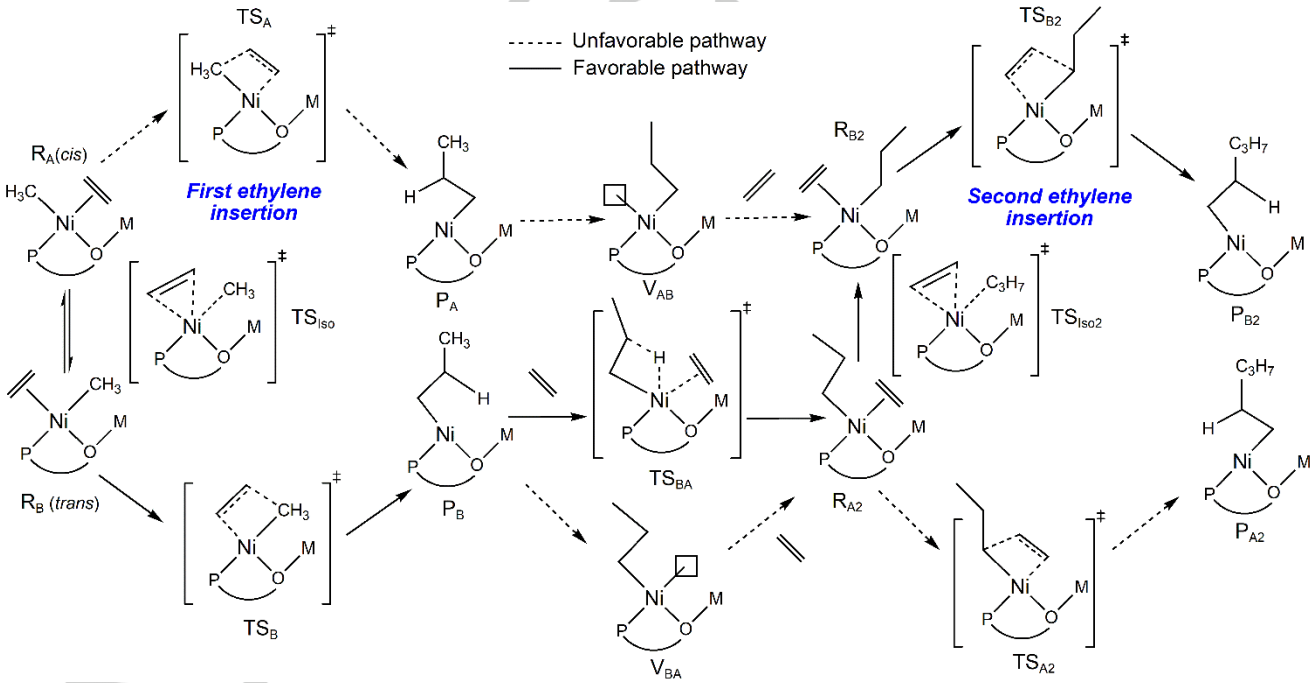

Scheme 1. Reaction mechanism for ethylene polymerization catalyzed by Ni-PEG with alkali metals (M^+). "Favorable pathway" is a plausible one in the present study.

Results and Discussion

Reaction pathways of Ni-PEG(M^+) for ethylene polymerization

In this work, DFT calculations were employed herein to comprehensively examine our proposed mechanism for ethylene polymerization catalyzed by Ni-PEG(M^+) as described by **Scheme 1.** Firstly, relative potential energy profiles for ethylene polymerization by each Ni-PEG(M^+) catalysts via favorable and unfavorable pathways were focused. Then, favorable pathways of heterobimetallic Ni-PEG with four alkali metals (M^+) were assessed. Finally, computed activation energies ($E_{a1(A-B)}$) from the favorable pathway of four Ni-PEG(M^+) systems were compared with a logarithm of activity from the experimental results [29]. In addition, the Gibbs free energy barrier ($\Delta G^{\ddagger}$) of the four Ni-PEG(M^+) systems were calculated to validate the $E_{a1(A-B)}$ from the potential energy calculations.

Favorable and unfavorable pathways of Ni-PEG(M^+)

The relative potential energy profiles of both favorable and unfavorable pathways for ethylene polymerization catalyzed by Ni-PEG(Li^+), Ni-PEG(Na^+), Ni-PEG(K^+), and Ni-PEG(Cs^+) catalysts in the gas phase were displayed in **Figures S1, S4, S7, and S10** of the supplementary material, respectively. All optimized structures of intermediate and transition state structures of both favorable and unfavorable pathways catalyzed by Ni-PEG with Li^+, Na^+, K^+, and Cs^+ are given in **Figures S2-S3, S5-S6, S8-S9** and **S11-S12**, respectively, in the supplementary material. The R_A was used as a starting structure for both favorable and unfavorable pathways for all four systems. For unfavorable pathway activation energies for the forward reaction along with R_A to P_A via TS_A ($E_{a1(A)}$) of Ni-PEG with Li^+, Na^+, K^+, and Cs^+ are 22.4, 17.9, 18.9, and 19.7 kcal mol^{-1}, respectively. These calculations suggested that the pathways require high activation energy. Thus, the isomerization step, which is included in the favorable pathway, is necessary, and the reaction is easily forwarded along with R_B to P_B via TS_B which requires the lower activation energy. Activation energies of the second ethylene insertion ($E_{a2(A)}$) of Ni-PEG with Li^+, Na^+, K^+, and Cs^+ are 18.6, 16.7, 20.1, and 21.0 kcal mol^{-1}, respectively. These results also showed that the unfavorable pathway involves high energy barriers, hence, these pathways should be excluded for the Ni-PEG(M^+) catalysts. In addition, the stability of P_A complexes is less than P_B for both first and second ethylene insertions. The β-agostic product has been identified as the resting state before the second ethylene insertion for several complexes of olefin polymerizations [41-42]. There is a possibility for P_A or P_B structure to generate a vacant site complex (V_{AB} or V_{BA}) via an unstable tri-coordinated structure before the new second ethylene insertion in R_B and R_A is formed. However, the result in a previous study [36] and also ours indicated that the vacant site complex would be difficult to generate because of the high activation energy being required in this process. For the favorable pathway, the P_B is continuously connected to the second ethylene insertion with the β-hydrogen elimination (TS_{BA}) which needs lower activation energy to form the stable R_{A2}. Then, the process of the forward reaction is similar to the first ethylene insertion which passes through TS_{Iso2}, R_{B2}, TS_{B2}, and P_{B2}.

Second metal effect on the favorable pathways

In the previous part, the details of the favorable pathway of Ni-PEG(M^+) were shown. Here, the effect of the second metal is discussed. The relative potential energy profiles of the favorable pathway of four Ni-PEG(M^+) catalytic systems are shown in **Figure 1**.

From the starting complex R_A of the first ethylene insertion, the isomerization of the Ni complex generates a reactive complex R_B. The R_B complex for $M^+ = Li^+$ is more stable than those for $M^+ = Na^+$, K^+, and Cs^+ by 2.1, 3.8, and 5.6 kcal mol^{-1}, respectively. This relative stability of the reactant π-complex corresponds to that obtained by Ziegler et al. in their study of the elementary reactions and the mechanism of polyethylene synthesis catalyzed by Ni complexes [39, 43]. The activation energy for the isomerization from R_A to R_B ($E_{a(Iso1)}$) is 7.7, 15.1, 18.3, and 19.5 kcal mol^{-1} for $M^+ = Li^+$, Na^+, K^+ and Cs^+, respectively. Then, the reaction proceeds along with R_B to P_B via TS_B with small activation energy ($E_{a1(B)}$). This is due to the less steric hindrance for the ethylene insertion into the *trans* position to the oxygen. The present result agrees with those reported by Nakano and Morokuma et al. [36] with the palladium phosphine-sulfonate catalysts. Because the reaction starting complex R_A is the more stable reactant, the energy difference between TS_B and R_A is defined as the activation energy ($E_{a1(A-B)}$). The $E_{a1(A-B)}$ is 7.0, 10.1, 11.5, and 12.9 kcal mol^{-1} for Ni-PEG with Li^+, Na^+, K^+, and Cs^+, respectively, which is closed to values reported by Imai et al [44]. The reaction energy (ΔE_{r1}), an energy difference between P_B and R_A, was calculated to be -24.6, -17.0, -15.2 and -12.6 kcal mol^{-1} for $M^+ = Li^+$, Na^+, K^+ and Cs^+, respectively. The ΔE_{r1} showed that the first ethylene insertion step is an exothermic process which is similar to that obtained from the previous DFT study for the reaction mechanism of the palladium-catalyzed ethylene polymerization by Morokuma group [45]. The R_A to P_B reaction with Ni-PEG(Li^+) is the most exothermic when compared with the others three alkali metal systems. This is because the distance between secondary metal (M^+) and oxygen of the PEG group (M-O_{PEG}) in the Li^+ system significantly decreases when the reaction proceeds from R_A to P_B. The average M-O_{PEG} distance in the R_A state is 2.17 Å, which is shrunk to 2.06 Å in the P_B state. Hence, the compactness of the PEG group in Ni-PEG(Li^+) is higher than in other alkali metals (see **Table S1** in the supplementary material).

Activation energies from P_B to R_{A2} via TS_{BA}(E_{a12}), β-hydrogen elimination step, for complexes with $M^+ = Li^+$, Na^+, K^+, and Cs^+ were found to be 7.2, 6.5, 5.9 and 3.4 kcal mol^{-1}, respectively. Thus, with Ni-PEG(Cs^+) the reaction is the easiest to be forwarded to R_{A2} because it has the smallest activation energy. The process is continued from R_{A2} to P_{B2} in a similar manner to the first ethylene insertion. For the second ethylene insertion, in the respective order for Ni-PEG with Li^+, Na^+, K^+, and Cs^+, the activation energy for the isomerization, $E_{a(Iso2)}$, is 5.9, 9.7, 15.0, and 17.5 kcal mol^{-1}, the activation energy to TS_{B2} from R_{A2} state, $E_{a2(A-B)}$, is 4.4, 6.3, 8.6, and 11.4 kcal mol^{-1}, and the reaction energy from R_{A2} to P_{B2}, ΔE_{r2}, is -25.2, -22.6, -17.5, and -14.3 kcal mol^{-1}. Trends for $E_{a(Iso2)}$ and $E_{a2(A-B)}$ in the second ethylene insertion are similar to those for $E_{a(Iso1)}$ and $E_{a1(A-B)}$ in the first insertion. However, the values for the second insertion are less. In addition, the trend of ΔE_{r2} is similar to ΔE_{r1}, in which longer alkyl groups provide more exothermic reaction by 1.3 (Li^+) to 5.6 (Na^+) kcal mol^{-1}.

Based on the relative potential energy profiles in **Figure 1**, the $E_{a(Iso1)}$ provided the highest energy barrier for ethylene polymerization catalyzed by Ni-PEG(M^+) for all the systems. Thus, the isomerization step is the rate-determining step of this reaction. This is consistent with the experimental results, i.e. the preference of isomer A for Ni-PEG(Li^+) and Ni-PEG(Cs^+) and the preference of isomer B for Ni-PEG(Na^+) and Ni-PEG(K^+). However, our calculation models for the reaction pathway are different from the pre-reaction model. Our calculations indicated that the ethylene insertion into the *cis* position to the oxygen is favored over its isomer, which agrees with those reported by Nozaki et al. [36] and Ziegler et al. [39]. Hence, the R_A is more stable than R_B for all Ni-PEG(M^+) systems. The trans-directing effect suggested that the polymerization reaction preferred ethylene insertion into the *trans* position to the oxygen could provide less steric hindrance [39]. Therefore, the isomerization step is always required for Ni-PEG(M^+) before the polymerization reaction takes place. While previous studies [45-46] have reported that the first ethylene insertion is the rate-determining step for the ethylene polymerization reaction, those works, however, did not include the isomerization step. To study the preference of isomer on M^+ cation, the $E_{a1(A-B)}$ which refers to the activation energy from R_A to polymerization reaction via TS_B including isomerization step was used to compare with experimental activities [29]. This comparison was given in the next section.

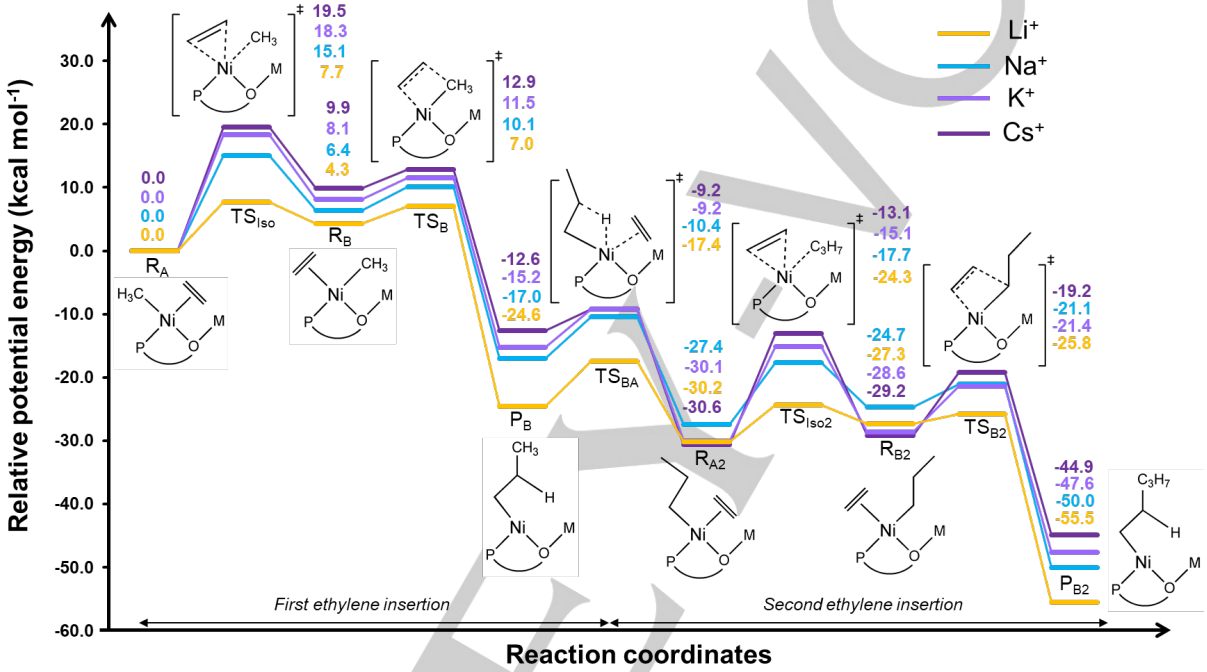

Figure 1. Relative potential energy profiles for ethylene polymerization catalyzed by Ni-PEG. Favorable pathways for alkali metals (M^+ = Li^+, Na^+, K^+, and Cs^+) were compared. Calculations were performed in the gas phase (see the solvent effect and Gibbs energy correction in **Figure S13** of supplementary materials). Each transition state and intermediate are designated in the proposed reaction pathway (**Scheme 1**). The potential energies relative to the complex R_A are given in kcal mol^{-1}.

Comparison of the DFT calculations and the experimental activities

According to the experiment, the trend of activities of the Ni-PEG catalysts with alkali metals (M^+) is in the order of Li^+ > Na^+ > K^+ > Cs^+ [29]. The low activation energy barrier in chemical reactions could provide better activity of the catalytic system [47-48]. **Table 1** showed the comparison of experimental activities and the result of our DFT calculations. The trend of $E_{a1(A-B)}$ of the favorable pathway of Ni-PEG was calculated to be Li^+ < Na^+ < K^+ < Cs^+. Hence, the DFT result agrees well with the activity trend from experiments. In addition, the Gibbs free energy barrier ($\Delta G^‡$) of four Ni-PEG(M^+) systems were also calculated and compared as shown in **Table 1**. The DFT trend obtained from Gibbs free energy barrier ($\Delta G^‡$) is similar to the activation energy barrier $E_{a1(A-B)}$ from the potential energy calculations. The correlation to the logarithm of activity is reasonable for both $E_{a1(A-B)}$ and $\Delta G^‡$ in **Table 1** [29]; R^2 = 0.73 for $\Delta G^‡$ and R^2 = 0.83 for $E_{a1(A-B)}$. In the following, the structure of R_A and TS_B were further analyzed to investigate the role of secondary metals (M^+) in Ni-PEG catalysts. Moreover, we described that the Ni-PEG(Li^+), which shows the lowest $E_{a1(A-B)}$, tends to be a good model for designing a high potential catalyst.

Table 1. Comparison of the experimental activities and our DFT calculation results.

Ni-PEG(M^+)	Experimental results [29]		DFT calculation results	
	Activity (kg mol^{-1} h^{-1})	log activity	$E_{a1(A-B)}$ (kcal mol^{-1})	$\Delta G^‡$ (kcal mol^{-1})
Li^+	35000	4.54	7.0	9.1
Na^+	18000	4.26	10.1	11.6
K^+	2900	3.46	11.5	12.8
Cs^+	360	2.56	12.9	13.2

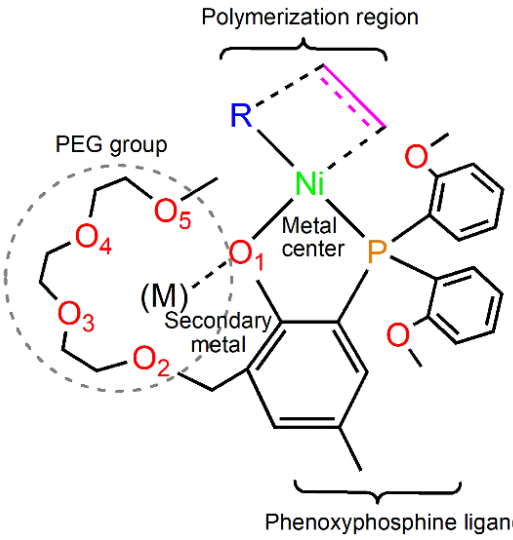

Figure 2. Structural classification of Ni-PEG with alkali metals (M^+ = Li^+, Na^+, K^+, and Cs^+). R = CH_3, C_3H_7 as growing chain for the first and the second ethylene insertion, respectively.

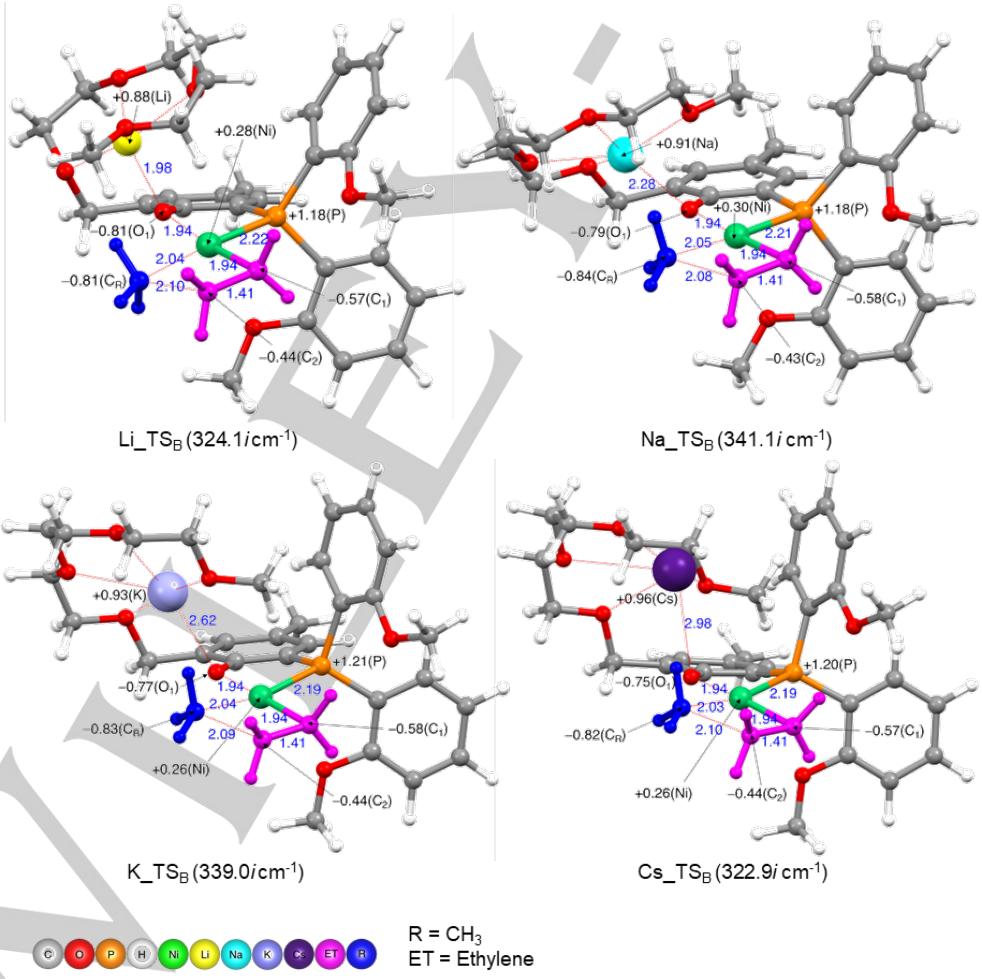

Figure 3. Optimized structure of transition state (TS_B) for ethylene polymerization by Ni-PEG catalysts with different alkali metals (M^+) for the first ethylene insertion (R = CH_3) of the favorable pathway. Distances (Å) are given in blue and NBO charges are shown in black.

Role of secondary metals (M^+) for ethylene polymerization

To understand the role of secondary metals related to the polymerization mechanism**.** The structure of Ni-PEG(M^+) was classified into 5 regions; nickel (Ni) metal center, polymerization region, phenoxyphosphine ligand, PEG group, and secondary metal (M^+) as represented in **Figure 2**.

Analysis of the role of M^+ at Ni-metal center and polymerization region

The Ni-metal center plays a crucial role in ethylene (ET) polymerization. Hence, the interaction around Ni with the polymerization region was firstly determined. Optimized structures of the four-membered ring transition state (TS_B) for ethylene polymerization by the Ni-PEG catalysts with different alkali metals (M^+) for the first ethylene insertion (R = CH_3) of the favorable pathway are given in **Figure 3**. Bond distances and NBO charges were analyzed for both steric and electronic effects in four Ni-PEG(M^+) catalytic systems.

In this section, we investigated the correlation between key parameters on polymerization region such as Ni-CH_3, Ni-P, ET-CH_3, Ni-ET, and Ni-O_1 distances and experimental activities of the four Ni-PEG(M^+) catalytic systems. From the analysis of the polymerization region, the Ni-CH_3 bond distances of four Ni-PEG(M^+) range from 2.03 to 2.05 Å. The Ni-P and ET-CH_3 distances are in the range of 2.19 – 2.22 Å and 2.08 – 2.10 Å, respectively. The Ni-ET and Ni-O_1 distances are approximately 1.94 Å, and no visible change was observed. Moreover, the NBO charges around the four-membered ring were also investigated for the TS_B state. The NBO charges of Ni, ET(C_1), ET(C_2), CH_3(C_R), O_1, and P are insensitive to M^+, with their average values of +0.28, –0.57, –0.44, –0.82, –0.78, and +1.19, respectively. However, no clear correlation was observed in the structural and electronic parameters for the Ni-metal center and polymerization region.

Analysis of the role of M^+ on metal-metal and metal-ligand interaction

The metal-metal and metal-ligand interactions were introduced to explain the cooperative heterobimetallic catalysts in different platforms [15]. In a previous study [24], it has been demonstrated that the addition of M^+ to NiL (L is phenoxyligand) can increase the catalytic efficiency up to 20 fold as well as polymer molecular weight and branching frequency in comparison to those without coadditives. This is because the enhancement of the electrophilicity of the nickel center and/or the steric/bulkiness of phenoxyimine ligand caused by alkali cations (Li^+, Na^+, and K^+) affects the ethylene insertion. However, there is no clear evidence for the origin of the steric and electronic effects on catalyst structures [24]. In this part, the metal-metal and metal-ligand interactions were investigated. The Ni and alkali metals (M^+) are connected via O_1 of the phenoxyphosphine ligand. Therefore, we examined the steric and electronic effects by analysis of the Ni-O_1, Ni-M, and M-O_1 bond distances and the NBO charges on Ni, O_1, and M^+ (Li^+, Na^+, K^+, and Cs^+) as given in **Figure 4.**

From analysis, the order is as follows: Ni-Li(3.48 Å) < Ni-Na(3.51 Å) < Ni-K(3.77Å) < Ni-Cs(3.89 Å) for Ni-M distance and Li-O_1(1.98 Å) < Na-O_1(2.28 Å) < K-O_1(2.62 Å) < Cs-O_1(2.98 Å) for M-O_1 distance. While the Ni-O_1 distance is equal to 1.94 Å for all the Ni-PEG(M^+) systems. Moreover, the trend of NBO charges on M^+ atom is Li^+(+0.88) < Na^+(+0.91) < K^+(+0.93) < Cs^+(+0.96). Interestingly, when using Li^+ as a secondary metal, the charge of O_1 atom show more negative value (–0.81) when compare with O_1 charge on Na^+(–0.79), K^+(–0.77), and Cs^+(–0.75).

The Ni-O_1-Li interaction was firstly examined because the Ni-Li complex has been proven to be the most active for Ni-PEG(M^+) catalysts [29]. The Ni-Li and Li-O_1 distances suggested that Ni is induced to cooperate the polymerization (through direct (Ni-Li) and indirect metal-metal (Ni-O_1-Li) interactions) by Li^+ better than other alkali metals. The shortest distance of Ni-O_1-Li (3.92 Å) indicates the strongest interaction between metal-metal and metal-ligand; on the contrary, the Ni-O_1-Cs exhibits the weakest interaction (Ni-O_1-Cs = 4.92 Å). Remarkably, we found a high correlation between Ni-O_1-M distance and the experimental activities of four Ni-PEG(M^+) catalytic systems which hints at a vital role of the secondary metal (M^+) on metal-metal and metal-ligand interactions. Moreover, the trend of NBO charge on M^+ shows good agreement with experimental activities. For instance, the most active catalyst has a less positive charge on M^+ (+0.88 for Li^+) while the least active catalyst has a more positive charge (+0.96 for Cs^+).

As evidenced by strong/weak interactions between metal-metal, the Ni-M interaction suggests the significance of the cooperative effect in Ni-PEG(M^+) catalysts. The positive NBO M^+ charge on the cation tends to be affected by the metal-ligand interaction since there are four oxygen atoms of PEG group surrounding the secondary metal. The interaction between M^+ and PEG group might affect the charge on M^+ and possibly relates to the rate of polymerization. Thus, the interaction between M^+ and PEG group was investigated in the next section.

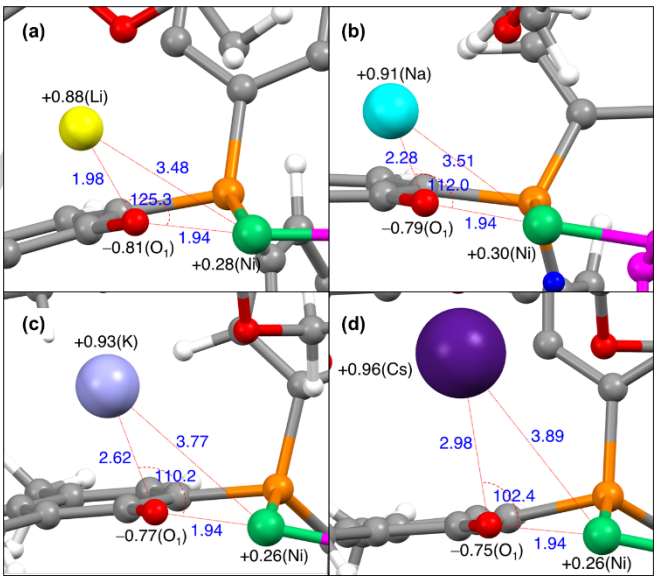

Figure 4. Bond distance (Å), bond angle (deg), and atomic charges of the optimized TS_B structure of Ni-PEG with (a) Li^+ (b) Na^+ (c) K^+, and (d) Cs^+. Distances and angles are given in blue, and NBO charges are shown in black. Those for the other atoms were omitted for clarity.

Analysis of the role of M^+ cation on PEG group

The secondary metal is cooperative with the primary metal to enhance the reactivity of ethylene polymerization for late transition metal catalysts [15]. According to a previous study, the PEG chain encapsulates the alkali cation (Na^+ and K^+) for steric shielding and provides Lewis acid sites. In which, they influence the catalyst activity and polymer morphology. By design, the PEG group is specifically provided the binding site for the alkali metal which assists the coordination-insertion polymerization. However, the theoretical insight on this phenomenon is still lacking [25]. In the Ni-PEG catalyst, the secondary metals have no direct interaction with nickel, but they could impact both the structure and electronic environment of the catalysts. Another study suggested that the flexible PEG group could coordinate Ni center and possibly hinder the reaction [29]. However, we found that the linear form of the alkyl PEG group, which can coordinate to the Ni center, is 14.5 kcal mol^{-1} less stable than the cyclic form as shown in **Figure S14** of the supplementary material. The results indicated that the compactness of the PEG group can increase the stability of the catalyst even though no second metal is coordinated to the PEG group. Therefore, the secondary metal in the Ni-PEG catalyst possibly controls the PEG group to stabilize the catalyst structure.

In this part, we focused on the interaction between M^+ and oxygens of the PEG group which is illustrated in **Figure 5**. The average distance between M^+ and four oxygens (O_2-O_5) of the PEG group (M-O_{PEG}) is 2.15, 2.42, 2.76, and 3.11 Å for M^+ = Li^+, Na^+, K^+, and Cs^+, respectively. The M^+ is located at the center of the PEG group to stabilize the positive charge by the four coordinating oxygens. It can be seen that the Li^+ has the shortest M-O_{PEG} distance, which implies that Li^+ can better control the PEG group in a compact space than the other alkali metals (Na^+, K^+, and Cs^+).

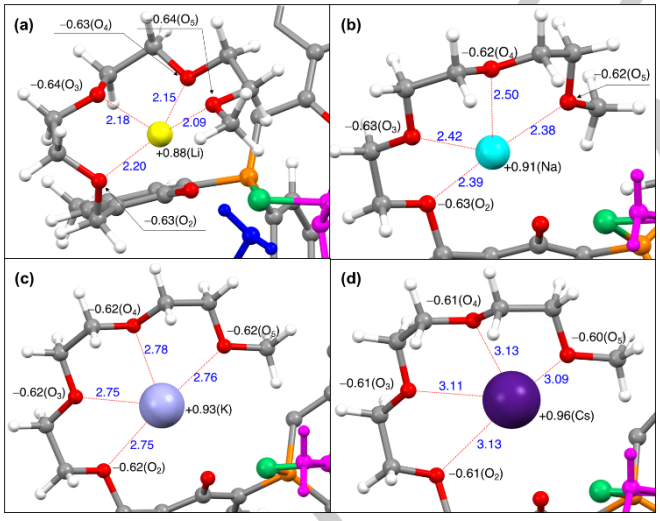

Figure 5. Optimized structure of Ni-PEG(M^+) in TS_B for the favorable pathway. Distances (Å) are given in blue and NBO charges are shown in black. The other atoms were omitted for clarity.

The interaction between M^+ and the PEG group can be determined from the binding energy. Binding energies of M^+ cation and PEG group were calculated and given in **Table S2** of the supplementary material. The result clearly showed that Li^+ exhibited the strongest interaction (the most stable). Moreover, we have examined the importance of the structure of the PEG framework on the activation energy ($E_{a1(A\text{-}B)}$) by changing M^+ cation. The Ni-Cs complex was modified by replacing Cs^+ with Li^+ and then performed the single-point calculations for the R_A, TS_B, and P_B states. The result for Ni-PEG(Li^+) with the Ni-PEG(Cs^+) structure, denoted by [Ni-PEG(Li^+):Ni-PEG(Cs^+)], is similar to that for Ni-PEG(Cs^+). For [Ni-PEG(Li^+):Ni-PEG(Cs^+)], $E_{a1(A\text{-}B)}$ and ΔE_r are 11.64 and -13.98 kcal mol^{-1}, respectively, which are comparable to those for Ni-PEG(Cs^+) ($E_{a1(A\text{-}B)}$ = 12.90 and ΔE_r = -12.60 kcal mol^{-1}). Thus, the PEG conformation is controlled by the M^+ cation and the structure of PEG is a key issue in controlling the rate of polymerization. (see more details in **Table S3** of the supplementary material).

To explain how the PEG group affects the activation energy ($E_{a1(A\text{-}B)}$), the average bond distance (Å) between the Ni-metal center and oxygens of the PEG group (Ni-O_{PEG}) were analyzed for the R_A and TS_B states. The result is given in **Figure S15** of the supplementary material. The results revealed that the Ni-O_{PEG} distance for the Li^+ case is 4.73 Å for R_A and decreases to 4.45 Å for TS_B. In contrast, the Ni-O_{PEG} distance for the Cs^+ case is 5.23 Å for R_A and slightly increases to 5.30 Å for TS_B. For Ni-PEG with Na^+ and K^+, only a slight reduction (around 0.1 Å) of the Ni-O_{PEG} distance from R_A to TS_B was observed. The lowest $E_{a1(A\text{-}B)}$ of Ni-PEG(Li^+) could be interpreted by the good ability of Li^+ to allow the PEG group to stabilize the transition state during the reaction whereas no significant structural rearrangement was observed in the cases of Ni-PEG(Na^+), Ni-PEG(K^+), and Ni-PEG(Cs^+).

The electrostatic effect of the secondary metal in Ni-PEG(M^+) was also analyzed via NBO charges. The NBO charges for M^+ are in the order Li^+ (+0.88) < Na^+ (+0.91) < K^+ (+0.93) < Cs^+ (+0.96). The average charges of the four oxygen (O_2-O_5) atoms of the PEG(M^+) group are –0.63, –0.62, –0.62, and –0.61 for Li^+, Na^+, K^+, and Cs^+, respectively. The Ni-Li complex exhibits a less positive charge when combined with the PEG group due to the charge transfer from Li^+ to oxygen atoms. This trend gradually decreases in the order of Ni-Li, Ni-Na, Ni-K, and Ni-Cs complexes, analogous to the increase of the ionization potential of M^+ (Li^+ < Na^+ < K^+ < Cs^+) [49].

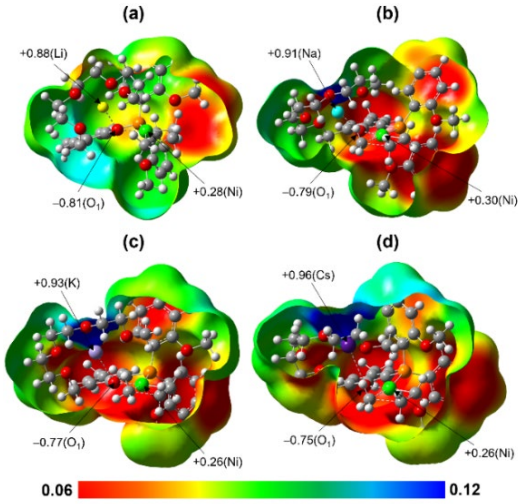

Figure 6. The molecular electrostatic potential (MEP) maps and NBO charges of M^+, O_1, and Ni atoms of the transition state (TS_B) Ni-PEG with (a) Li^+ (b) Na^+ (c) K^+, and (d) Cs^+. The isosurface

value is 0.002 with a range for the MEPs map of 0.06 to 0.12 a.u. for all systems.

Molecular Electrostatic Potential (MEP) map was applied to analyze the electrostatic effect in this work. The MEP maps and NBO charges of M^+, O_1, and Ni atoms at the transition state (TS_B) Ni-PEG with Li^+, Na^+, K^+, and Cs^+ are presented in **Figure 6a-d**, respectively. The red color indicates the electron-rich or more negative charge region, whereas the blue color represents the electron-deficient or more positive charge region. We found that the order of blue-color intensity in the MEP corresponds to the NBO calculations. The Ni-Cs complex provides the more positive charge around the PEG group while the Ni-Li complex possesses the less positive charge. Thus, for M^+ in Ni-PEG(M^+) Li^+ is the least electropositive when compared to other alkali ions. Hence, with the presence of Li^+, the rate of polymerization could be enhanced by the reduction of positive charge around the PEG group.

For obtaining high-performance catalysts, the secondary metal should provide strong interactions for both direct (Ni-M) and indirect (Ni-O_1-M) metal-metal as well as metal-ligand (M-phenoxyphosphine and M-PEG group). Moreover, the less positive charge on M^+ of the PEG group can enhance the polymerization rate.

Influence of catalyst structures on experimental activity

Ni-PEG with M^+ cation

In the last section, we focused on the pre-reaction state of the Ni-PEG(M^+) catalysts. If there is a correlation between the structure of the pre-reaction state and experimental activity, the computational effort for a predictive study would be much less (in comparison with that of the transition state optimization). Initially, the relative stabilities of Ni-PEG with four alkali metal cations (M^+) with two different geometric isomers A and B were compared (see **Figure S16** in the supplementary material). Our results revealed that Ni-PEG with Li^+ and Cs^+ are more stable in isomer A, whereas those with Na^+ and K^+ are more stable in isomer B. This suggestion corresponds to the experimental finding on the existing ratio of the isomers A: B [29]. Then, we employed the most stable isomer to find the relationship between the catalyst structures and the experimental activities [29]. Selected bond lengths, bond angles, dihedral angles, and NBO charges of the optimized Ni-PEG(M^+) catalysts were presented in **Table S4** of the supplementary material.

From the analysis, we found the best two parameters, the distance between the secondary metal and O_1 of phenoxyphosphine ligand (M-O_1) and the average distance between M^+ and four oxygens (O_2-O_5 atoms) of the PEG group (M-O_{PEG}), with a high correlation to experimental activities [29]. The relationship between log(activity) and the M-O_1 and M-O_{PEG} distances was plotted in **Figure 7**. To assure a high level of correlation with experimental activity, a criterion for the R-square (R^2) with a value ≥ 0.8 was used [50-51]. From **Figure 7**, plots of the M-O_1 and M-O_{PEG} distances parameters with log(activity) showed R^2 of 0.98 and 0.97, respectively. Hence, these two key parameters could be used for the design and screening of the potent Ni-PEG catalysts. The two parameters are also highly correlated with R^2 of 0.99 between them. To summarize, the potent Ni-PEG catalysts should have shorter distances for M-O_1 and M-O_{PEG}. We, in addition, monitored the Ni charge and found that Ni-PEG with Li^+ also has the largest charge. The stronger Ni charge enhances ethylene attraction and polymerization activity.

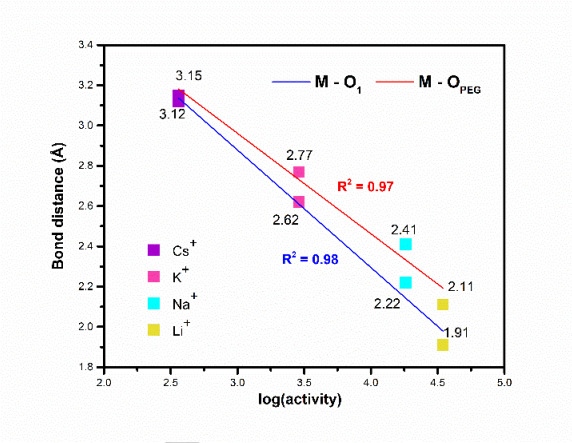

Figure 7. The relationship between log(activity) and the M-O_1 and M-O_{PEG} distances from the most stable isomer of Ni-PEG with four alkali metals (M^+ cation).

Potent Ni-PEG catalysts with M^{2+} cation

The Ni-PEG catalyst with Li^+ for the secondary metal is the most active catalyst among the alkali metals [29]. Our study has also revealed that the catalyst with the shorter M-O_{PEG} and M-O_1 distance has the more enhanced catalytic activity and that with Li^+ has the shortest distances, see **Figure 7**. It is, thus, interesting to use these geometrical parameters to predict the activity of Ni-PEG with other secondary metals such as the divalent cation, M^{2+}. Hence, the Ni-PEG(M^{2+}) with alkaline-earth metals (Be^{2+}, Mg^{2+}, Ca^{2+}, Sr^{2+}) and other divalent transition metals such as Co^{2+} and Zn^{2+} were investigated in the same way as the Ni-PEG(M^+) system (for the reason of the relative stability, see text below **Figure S17** of the supplementary material). We have also checked for the relative stability of the spin states for all the metals and found that the spin multiplicity of the Ni-PEG(M^{2+}) systems is singlet except for the Co^{2+} complex which is a quartet spin.

The optimized structures of Ni-PEG catalysts with M^{2+} cations (Be^{2+}, Mg^{2+}, Ca^{2+}, Sr^{2+}, Co^{2+}, and Zn^{2+}) were compared with the Ni-PEG(Li^+) complex and demonstrated in **Figures 8a-g**. The M-O_1 distances for Ni-PEG with Be^{2+}, Mg^{2+}, Ca^{2+}, Sr^{2+}, Co^{2+}, and Zn^{2+} are 1.59, 1.94, 2.32, 2.42, 1.91, and 1.89 Å, respectively. The M-O_{PEG} distances for Ni-PEG with Be^{2+}, Mg^{2+}, Ca^{2+}, Sr^{2+}, Co^{2+}, and Zn^{2+} are 1.85, 2.13, 2.47, 2.60, 2.17, and 2.13 Å, respectively. Calculated values for M-O_1 and M-O_{PEG} of Ni-PEG with Mg^{2+}, Co^{2+}, and Zn^{2+} are closed to those of Ni-PEG(Li^+). This suggests that the catalyst with Mg^{2+}, Co^{2+}, and Zn^{2+} as the secondary metal could also yield high activity. Interestingly, the Ni-PEG(Be^{2+}) exhibited the shortest distance for both M-O_1 and M-O_{PEG}. Thus, the PEG group in this catalyst is in the most compact form and shows the strongest metal-ligand interaction. Therefore, the Ni-PEG catalyst with Be^{2+} cation is the most promising candidate.

Recently, Xiao et al. [27] have reported that nickel complexes with phosphine phosphonate-PEG ligand in combination with Co^{2+} and Zn^{2+} cations can enhance the rate of polymerization. This finding agrees with our results. Our study, therefore, provided key concepts for designing highly active catalysts for ethylene polymerization based on the Ni-PEG.

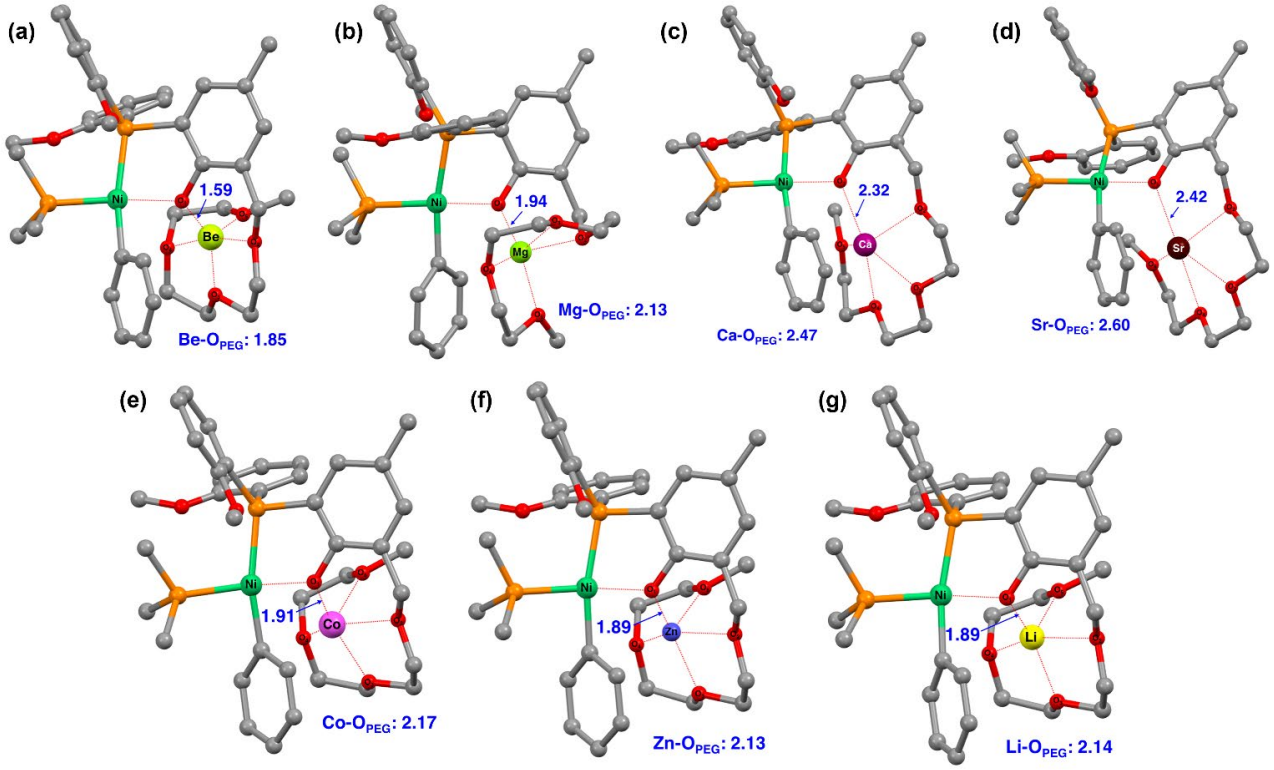

Figure 8. Optimized structures of the Ni-PEG catalysts with (a) Be^{2+} (b) Mg^{2+} (c) Ca^{2+} (d) Sr^{2+} (e) Co^{2+} and (f) Zn^{2+} cation. Their structures were compared with that of the most active (g) Ni-PEG(Li^{+}) catalyst. The bond distances (Å) are given in blue color and the H atoms are omitted for clarity.

Conclusion

In this study, we aimed to shed light on the possible reaction mechanism of heterobimetallic nickel phenoxyphosphine polyethylene glycol (Ni-PEG) catalysts with different alkali metals (M^{+}) for ethylene polymerization using DFT method. Obtained results from the potential energy profiles revealed that the isomerization step is the necessary step for this reaction. Moreover, the reactant π-complex with ethylene at *trans* to the oxygen provides low activation energy. We have found a good correlation between the experimental (log) activity of Ni-PEG(M^{+}) and the activation energy of the favorable pathway ($E_{a1(A\text{-}B)}$), $E_{a1(A\text{-}B)}$ of Ni-PEG(Li^{+}) < Ni-PEG(Na^{+}) < Ni-PEG(K^{+}) < Ni-PEG(Cs^{+}). Furthermore, the multiple roles of secondary metals (M^{+}) were elucidated. Importantly, this finding suggests that the highly active catalyst should have strong interactions for both direct (Ni-M) and indirect (Ni-O_1-M) metal-metal as well as metal-ligand (M-phenoxyphosphine and M-PEG group). Additionally, the catalyst with less positively charged M^{+} cation could enhance the polymerization rate. Besides, the key role of the secondary metal is to control the PEG group which stabilizes the catalyst structure. Two key parameters, i.e. M-O_1 and M-O_{PEG} distances, were found to have a high correlation with the experimental activities (R^2 > 0.8). Thus, potent Ni-PEG(M^{+}) catalysts have shorter M-O_1 and M-O_{PEG} distances. Hence, we employed these parameters to design and screen a potential candidate for Ni-PEG(M^{2+}) catalysts. Values of M-O_1 and M-O_{PEG} for the Ni-PEG with Mg^{2+}, Co^{2+}, and Zn^{2+} are similar to those of Ni-PEG(Li^{+}). Moreover, from values of two key parameters Ni-PEG(Be^{2+}) provides the best compactness of the PEG group, which indicates the strongest metal-ligand interaction. Therefore, we suggest the Ni-PEG(M^{2+}) catalysts with Be^{2+}, Mg^{2+}, Co^{2+}, and Zn^{2+} as the secondary metal for candidates of high activity catalysts. This work has provided fundamental insights into the reaction mechanism of the Ni-PEG(M^{+}) catalysts and clarified the role of the secondary metal. More importantly, the finding paves the way for the design and development of the Ni-PEG catalysts for ethylene polymerization.

Computational details

Computational models

Using X-ray structures of Ni-PEG with alkali metals [28-29], pre-reaction structures (**Figure 9**, left) with two different geometric isomers A and B were optimized, and their relative stabilities were compared for four kinds of Ni-PEG(M^{+}) catalytic systems as given in **Figure S16** of supplementary material. According to an experiment, phosphine abstraction is the first step in the activation process. From the ^{31}P NMR spectroscopy [29], the PMe_3 group can easily be removed from the nickel center, thus, it is possible to generate a vacant site for ethylene insertion there. Generally, the migratory insertion is responsible for the growth of the alkyl chain [35], while no evidence has been reported for the coordination with the phenyl group during polymerization [29]. In this study, we employed CH_3 and C_3H_7 for the R group as growing chains for the first and the second ethylene insertion, respectively. Thus, the ethylene insertion complex model (**Figure 9**, right) was constructed as a starting structure to study the reaction mechanism of the Ni-PEG(M^{+}) catalysts for ethylene polymerization. As mentioned in the introduction, according to a previous study [38], the counteranion does not have an impact on the reaction mechanism. To reduce the computation complexity,

models without counteranion and explicit solvents were employed in our calculations.

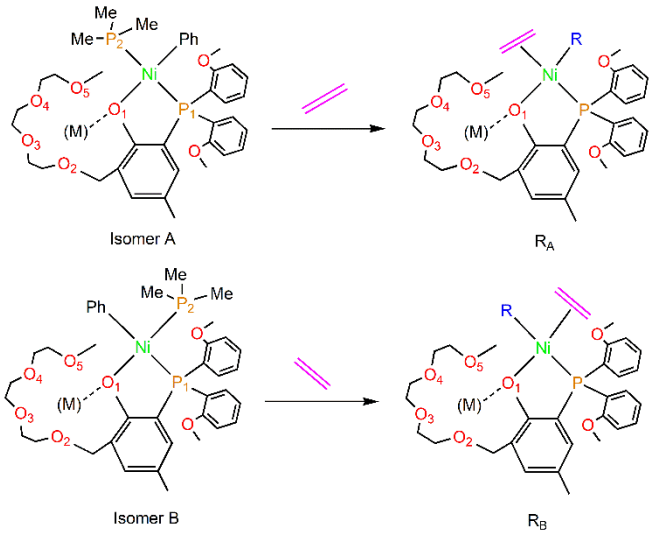

Figure 9. Heterobimetallic Ni-PEG with alkali metals (M^+ = Li^+, Na^+, K^+, and Cs^+) for pre-reaction model (left) and for reaction pathway model (ethylene insertion complex, right). The geometric isomer A (top) and B (bottom) were defined. R=CH_3 and R=C_3H_7 as a growing chain for the first and the second ethylene insertion, respectively.

Based on the proposed reaction mechanism in **Scheme 1**, the activation energy ($E_{a1(A\text{-}B)}$) was calculated according to Eq. (1):

$$E_{a1(A\text{-}B)} = E_{TS_B} - E_{R_A} \quad (1)$$

The $E_{a1(A\text{-}B)}$ for ethylene polymerization catalyzed by Ni-PEG with different alkali metals (M^+ = Li^+, Na^+, K^+, and Cs^+) was first determined to compare with Tran et al.'s experimental activities [29]. In addition, the activation energy for isomerization ($E_{a(Iso1)}$), the activation energy for the unfavorable route ($E_{a1(A)}$), the activation energy for the favorable route ($E_{a1(B)}$), reaction energy (ΔE_{r1}), and activation energy of the β-hydrogen elimination step (E_{a12}) were calculated for the first ethylene insertion according to Eq. (2) to Eq. (6), respectively. While Eq. (7) to Eq. (10) were used for the calculations of the second ethylene insertion.

$$E_{a(Iso1)} = E_{TS_{Iso}} - E_{R_A} \quad (2)$$

$$E_{a1(A)} = E_{TS_A} - E_{R_A} \quad (3)$$

$$E_{a1(B)} = E_{TS_B} - E_{R_B} \quad (4)$$

$$\Delta E_{r1} = E_{P_B} - E_{R_A} \quad (5)$$

$$E_{a12} = E_{TS_{BA}} - E_{P_B} \quad (6)$$

$$E_{a(Iso2)} = E_{TS_{Iso2}} - E_{R_{A2}} \quad (7)$$

$$E_{a2(A)} = E_{TS_{A2}} - E_{R_{A2}} \quad (8)$$

$$E_{a2(A\text{-}B)} = E_{TS_{B2}} - E_{R_{A2}} \quad (9)$$

$$\Delta E_{r2} = E_{P_{B2}} - E_{R_{A2}} \quad (10)$$

DFT calculations

All the calculations were carried out using the Gaussian16 (Rev.A.03) program [52]. Density Functional Theory (DFT) calculations were performed by using the ωB97XD functional [53-54] with 6-31G(d) basis set [55] for C, H, O, P, Li, Na, K, Be, Mg, Ca, Co, and Zn atoms and with the effective core potential (ECP) plus SDD basis set [56-57] for Ni, Sr, and Cs atoms. We have checked for the spin multiplicities of the ground states of the Ni complexes in this catalytic reaction. Our calculations found that all singlet state molecules are significantly more stable than the triplet states. Therefore, we believe the ethylene polymerization reaction catalyzed by the Ni-PEG(M^+) went through a low spin pathway. The optimized Ni-PEG(M^+) with different method/basis set were compared with the X-ray structures [28-29] (see **Tables S5-S6** in the supplementary material). All the optimized stationary and transition state structures were confirmed by zero and one imaginary frequency, respectively, in normal mode analysis. The process from reactant π-complex–TS–β-agostic product was verified by intrinsic reaction coordinate (IRC) calculations. The structures were calculated in gas phase condition and single-point calculations with the self-consistent reaction field (SCRF) method using the SMD solvation model [58-59]. The dielectric constant of toluene (Eps = 2.3741) was employed. The relative potential energies both in the gas phase and in the toluene solvent of Ni-PEG(Li^+) were calculated (see in **Figure S13** of supplementary material). For a comparison, relative potential energy profiles of four Ni-PEG(M^+) catalytic systems in the gas phase were shown in **Figure 1**. In addition, Gibbs free energy profile at 298.15 K in toluene solvent of the Ni-PEG(Li^+) catalyst was also calculated and reported in **Figure S13** of supplementary material. As only very minor corrections were given, we adopted potential energy profiles in the gas phase to study the second-metal effect. For the pre-reaction state, some selected key bond parameters in the optimized structures were examined to find the correlation between the catalyst structure and experimental activities. Moreover, natural population analysis (NPA) [60-61] was performed for the natural atomic charges (NBO) with Gaussian NBO Version 3.1.

Acknowledgements

P. A. acknowledge the financial support from the Development and Promotion of Science and Technology Talents Project (DPST). We are gratefully thankful to the Center of Excellence in Computational Chemistry (CECC), National e-Science Infrastructure Consortium and Institute for Catalysis (ICAT) at Hokkaido University for providing high performance computing services and facilities. M. R. and J. H. acknowledge the MEXT project of Integrated Research Consortium on Chemical Science (IRCCS).

Keywords: Heterobimetallic • Mechanism • Ethylene polymerization • DFT calculations • Catalyst design

[1] I. V. Sedov, V. D. Makhaev, P. E. Matkovskii, *Catal. Ind.* **2012**, *4*, 129-140.
[2] L. Lebreton, A. Andrady, *Palgrave Commun.* **2019**, *5*, 1-11.
[3] P. Cossee, *J. Catal.* **1964**, *3*, 80-88.
[4] A. Shamiri, M. H. Chakrabarti, S. Jahan, M. A. Hussain, W. Kaminsky, P. V. Aravind, W. A. Yehye, *Materials* **2014**, *7*, 5069-5108.
[5] J. Huang, G. L. Rempel, *Prog. Polym. Sci.* **1995**, *20*, 459-526.
[6] W. Kaminsky, A. Laban, *Appl. Catal. A: Gen.* **2001**, *222*, 47-61.
[7] M. Ratanasak, J. Hasegawa, V. Parasuk, *New J. Chem.* **2021**, *45*, 8248-8257.
[8] H. G. Alt, A. Köppl, *Chem. Rev.* **2000**, *100*, 1205-1222.
[9] B. Wang, *Coord. Chem. Rev.* **2006**, *250*, 242-258.
[10] M. C. Baier, M. A. Zuideveld, S. Mecking, *Angew. Chem. Int. Ed.* **2014**, *53*, 9722-9744.

[11] H. Makio, H. Terao, A. Iwashita, T. Fujita, *Chem. Rev.* **2011**, *111*, 2363-2449.
[12] J. Vela, G. R. Lief, Z. Shen, R. F. Jordan, *Organometallics* **2007**, *26*, 6624-6635.
[13] S. Zai, H. Gao, Z. Huang, H. Hu, H. Wu, Q. Wu, *ACS Catal.* **2012**, *2*, 433-440.
[14] X. Wang, Y. Zhang, F. Wang, L. Pan, B. Wang, Y. Li, *ACS Catal.* **2021**, *11*, 2902-2911.
[15] Z. Cai, D. Xiao, L. H. Do, *Comments Inorg. Chem.* **2019**, *39*, 27-50.
[16] S. Liu, A. Motta, A. R. Mouat, M. Delferro, T. J. Marks, *J. Am. Chem. Soc.* **2014**, *136*, 10460-10469.
[17] H. Chiu, A. Koley, P. L. Dunn, R. J. Hue, I. A. Tonks, *Dalton Trans.* **2017**, *46*, 5513-5517.
[18] B. G. Cooper, J. W. Napoline, C. M. Thomas, *Catal. Rev.* **2012**, *54*, 1-40.
[19] G. H. C. Masson, T. R. Cruz, P. D. S. Gois, D. M. Martins, B. S. Lima-Neto, G. S. Oliveira, A. E. H. Machado, K. Bernardo-Gusmão, B. E. Goi, V. P. Carvalho-Jr, *New J. Chem.* **2021**, *45*, 11466-11473.
[20] L. K. Johnson, C. M. Killian, M. Brookhart, *J. Am. Chem. Soc.* **1995**, *117*, 6414-6415.
[21] M. J. West, A. J. B. Watson, *Org. Biomol. Chem.* **2019**, *17*, 5055-5059.
[22] N. Hazari, P. R. Melvin, M. M. Beromi, *Nat. Rev. Chem.* **2017**, *1*, 0025.
[23] V. P. Ananikov, *ACS Catal.* **2015**, *5*, 1964-1971.
[24] Z. Cai, D. Xiao, L. H. Do, *J. Am. Chem. Soc.* **2015**, *137*, 15501-15510.
[25] Z. Cai, L. H. Do, *Organometallics* **2017**, *36*, 4691-4698.
[26] D. Zhang, C. Chen, *Angew. Chem. Int. Ed.* **2017**, *56*, 14672-14676.
[27] D. Xiao, Z. Cai, L. H. Do, *Dalton Trans.* **2019**, *48*, 17887-17897.
[28] T. V. Tran, Y. H. Nguyen, L. H. Do, *Polym. Chem.* **2019**, *10*, 3718-3721.
[29] T. V. Tran, L. J. Karas, J. I. Wu, L. H. Do, *ACS Catal.* **2020**, *10*, 10760-10772.
[30] E. Schiebel, M. Voccia, L. Falivene, L. Caporaso, S. Mecking, *ACS Catal.* **2021**, *11*, 5358-5368.
[31] M. D. Leatherman, S. A. Svejda, L. K. Johnson, M. Brookhart, *J. Am. Chem. Soc.* **2003**, *125*, 3068-3081.
[32] L. Deng, T. K. Woo, L. Cavallo, P. M. Margl, T. Ziegler, *J. Am. Chem. Soc.* **1997**, *119*, 6177-6186.
[33] D. G. Musaev, R. D. J. Froese, M. Svensson, K. Morokuma, *J. Am. Chem. Soc.* **1997**, *119*, 367-374.
[34] A. Zeller, T. Strassner, *J. Organomet. Chem.* **2006**, *691*, 4379-4385.
[35] S. Noda, A. Nakamura, T. Kochi, L. W. Chung, K. Morokuma, K. Nozaki, *J. Am. Chem. Soc.* **2009**, *131*, 14088-14100.
[36] R. Nakano, L. W. Chung, Y. Watanabe, Y. Okuno, Y. Okumura, S. Ito, K. Morokuma, K. Nozaki, *ACS Catal.* **2016**, *6*, 6101-6113.
[37] D. E. Ortega, D. Cortés-Arriagada, O. S. Trofymchuk, D. Yepes, S. Gutiérrez-Oliva, R. S. Rojas, A. Toro-Labbé, *Chem. Eur. J.* **2017**, *23*, 10167-10176.
[38] A. Laine, B. B. Coussens, J. T. Hirvi, A. Berthoud, N. Friederichs, J. R. Severn, M. Linnolahti, *Organometallics* **2015**, *34*, 2415-2421.
[39] M. S. W. Chan, L. Deng, T. Ziegler, *Organometallics* **2000**, *19*, 2741-2750.
[40] I. Ugi, D. Marquarding, H. Klusacek, P. Gillespie, F. Ramirez, *Acc. Chem. Res.* **1971**, *4*, 288-296.
[41] M. Brookhart, M. L. H. Green, G. Parkin, *Proc. Natl. Acad. Sci. U. S. A.* **2007**, *104*, 6908-6914.
[42] B. J. Burger, M. E. Thompson, W. D. Cotter, J. E. Bercaw, *J. Am. Chem. Soc.* **1990**, *112*, 1566-1577.
[43] A. Michalak, T. Ziegler, *Organometallics* **2003**, *22*, 2069-2079.
[44] H. Imai, H. Uchida, *Bull. Chem. Soc. Jpn.* **1967**, *40*, 321-326.
[45] D. G. Musaev, M. Svensson, K. Morokuma, S. Strömberg, K. Zetterberg, P. E. M. Siegbahn, *Organometallics* **1997**, *16*, 1933-1945.
[46] K. Vanka, Z. Xu, M. Seth, T. Ziegler, *Top. Catal.* **2005**, *34*, 143-164.
[47] B. Aguila, Q. Sun, X. Wang, E. O'Rourke, A. M. Al-Enizi, A. Nafady, S. Ma, *Angew. Chem. Int. Ed.* **2018**, *57*, 10107-10111.
[48] X. Feng, Y. Zhao, D. Liu, Y. Mo, Y. Liu, X. Chen, W. Yan, X. Jin, B. Chen, X. Duan, D. Chen, C. Yang, *Int. J. Hydrog. Energy* **2018**, *43*, 17112-17120.
[49] P. W. Atkins, J. De Paula, *Atkins' Physical chemistry*, tenth ed., Oxford University Press, Oxford, **2014**.
[50] T. Elder, J. J. Bozell, D. Cedeno, *Phys. Chem. Chem. Phys.* **2013**, *15*, 7328-7337.
[51] M. Ratanasak, T. Rungrotmongkol, O. Saengsawang, S. Hannongbua, V. Parasuk, *Polymer* **2015**, *56*, 340-345.
[52] M. J. Frisch, G. W. Trucks, H. B. Schlegel, G. E. Scuseria, M. A. Robb, J. R. Cheeseman, G. Scalmani, V. Barone, G. A. Petersson, H. Nakatsuji, X. Li, M. Caricato, A. V. Marenich, J. Bloino, B. G. Janesko, R. Gomperts, B. Mennucci, H. P. Hratchian, J. V. Ortiz, A. F. Izmaylov, J. L. Sonnenberg, Williams, F. Ding, F. Lipparini, F. Egidi, J. Goings, B. Peng, A. Petrone, T. Henderson, D. Ranasinghe, V. G. Zakrzewski, J. Gao, N. Rega, G. Zheng, W. Liang, M. Hada, M. Ehara, K. Toyota, R. Fukuda, J. Hasegawa, M. Ishida, T. Nakajima, Y. Honda, O. Kitao, H. Nakai, T. Vreven, K. Throssell, J. A. Montgomery Jr., J. E. Peralta, F. Ogliaro, M. J. Bearpark, J. J. Heyd, E. N. Brothers, K. N. Kudin, V. N. Staroverov, T. A. Keith, R. Kobayashi, J. Normand, K. Raghavachari, A. P. Rendell, J. C. Burant, S. S. Iyengar, J. Tomasi, M. Cossi, J. M. Millam, M. Klene, C. Adamo, R. Cammi, J. W. Ochterski, R. L. Martin, K. Morokuma, O. Farkas, J. B. Foresman, D. J. Fox, *Gaussian 16 Rev. A.03* **2016**.
[53] J.-D. Chai, M. Head-Gordon, *Phys. Chem. Chem. Phys.* **2008**, *10*, 6615-6620.
[54] S. Grimme, *WIREs Comput. Mol. Sci.* **2011**, *1*, 211-228.
[55] K. E. Riley, K.-A. Tran, P. Lane, J. S. Murray, P. Politzer, *J. Comput. Sci.* **2016**, *17*, 273-284.
[56] A. Posada-Borbón, A. Posada-Amarillas, *Chem. Phys. Lett.* **2015**, *618*, 66-71.
[57] W. G. Xu, B. Jin, *Chem. Phys. Lett.* **2006**, *419*, 439-443.
[58] S. Miertuš, E. Scrocco, J. Tomasi, *Chem. Phys.* **1981**, *55*, 117-129.
[59] A. V. Marenich, C. J. Cramer, D. G. Truhlar, *J. Phys. Chem. B* **2009**, *113*, 6378-6396.
[60] A. E. Reed, F. Weinhold, *J. Chem. Phys.* **1983**, *78*, 4066-4073.
[61] A. E. Reed, R. B. Weinstock, F. Weinhold, *J. Chem. Phys.* **1985**, *83*, 735-746.

Table of Contents

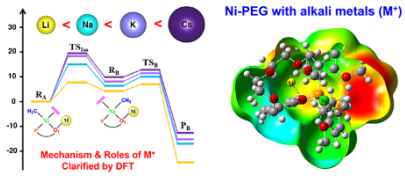

To shed light on the possible reaction mechanism of heterobimetallic nickel phenoxyphosphine polyethylene glycol (Ni-PEG) catalysts with different alkali metals (M^+) for ethylene polymerization using DFT method. The trend of activation energies ($Li^+ < Na^+ < K^+ < Cs^+$) shows good agreement with experimental activities. The multiple roles of secondary metals (M^+) were elucidated.

WILEY-VCH